



# ECE Imaging System in LHD

Daiki Nishimura<sup>1</sup> · Tokihiko Tokuzawa<sup>1,2,3</sup> · Daisuke Kuwahara<sup>4</sup> · Tatsuhiro Nasu<sup>2</sup>

Received: 14 July 2025 / Accepted: 13 December 2025  
© The Author(s) 2025

## Abstract

Electron Cyclotron Emission Imaging(ECEI) is a powerful tool for investigating MHD instabilities and turbulence in magnetically confined plasma. In the LHD, the ECEI system has been developed and successfully obtained two-dimensional images of temperature fluctuations. This paper describes the current V-band and Q-band ECEI systems including developments in their key components. The initial results of the observation of geodesic acoustic mode (GAM) are presented.

**Keywords** ECE imaging · Temperature fluctuations · GAM

## Introduction

Electron cyclotron emission imaging (ECEI) enables visualization of the spatial structure of electron temperature fluctuations in magnetically confined plasma. It has proven to be a powerful diagnostic tool for investigating instabilities in fusion plasma experiments, and its underlying technology has been continuously improved [1, 2]. ECE intensity is proportional to the electron temperature in optically thick plasma, and the emission frequency reflects the local magnetic field strength. Therefore, ECE measurements can provide the local electron temperature along the radial direction. The ECE diagnostic is used in fluctuation and transport studies due to its high temporal resolution. ECEI can obtain the two-dimensional electron temperature distribution and its fluctuations in a poloidal cross-section achieved by vertically aligning ECE detector array. Since the pioneering observation of sawtooth crashes with ECEI on TEXTOR [3], ECEI have been installed on tokamaks such as DIII-D,

KSTAR, ASDEX-Upgrade, and HL-3 [4–7], where they have succeeded in clarifying the structures of Alfvén eigenmodes [8], tearing modes [9], and edge-localized modes [10]. ECEI can be implemented on helical devices based on essentially the same concept as in tokamaks. In LHD, a W-band ECEI system combined with microwave imaging reflectometry was previously developed [11]. In this paper, we introduce the newly installed V- and Q-band ECEI systems [12, 13]. These systems are designed to target MHD modes [14] and geodesic acoustic modes (GAMs) [15] that are observed in plasmas with relatively low toroidal magnetic field configurations ( $B_t = 1.0\text{--}1.375\text{ T}$ ). We developed two V-band modules and Q-band module to detect second-harmonic ECE signal. The development of the three modules has made it possible to perform observations over wide experimental parameters. Figure 1 shows the corresponding measurement regions of the V- and Q-band receiver in major radius for typical low- magnetic field configurations with magnetic axis positions  $R_{ax} = 3.60\text{ m}$  and  $R_{ax} = 3.75\text{ m}$ . The observation region of the V-band receiver includes the  $\iota/2\pi = 0.5$  rational surface, whereas that of the Q-band module includes the  $\iota/2\pi = 1.0$  rational surface. The new ECEI system is installed at the 4-O port of LHD and uses a five-mirror optical system to transmit and focus the ECE radiation onto three heterodyne radiometer modules equipped with Local oscillator Integrated Antenna (LIA). Each module has eight vertically aligned antennas, and the received signals are down-converted to an intermediate frequency and divided into eight frequency channels by a filter-bank system, providing 64 spatial channels per module.

✉ Daiki Nishimura  
nishimura.daiki@nifs.ac.jp

<sup>1</sup> National Institute for Fusion Science, National Institutes of Natural Sciences, Toki 509-5292, Gifu, Japan

<sup>2</sup> The Graduate University for Advanced Studies, SOKENDAI, Toki 509-5292, Gifu, Japan

<sup>3</sup> Research Institute for Applied Mechanics, Kyushu University, Kasuga 816-8580, Fukuoka, Japan

<sup>4</sup> College of Science and Engineering, Chubu University, Kasugai 487-8501, Aichi, Japan

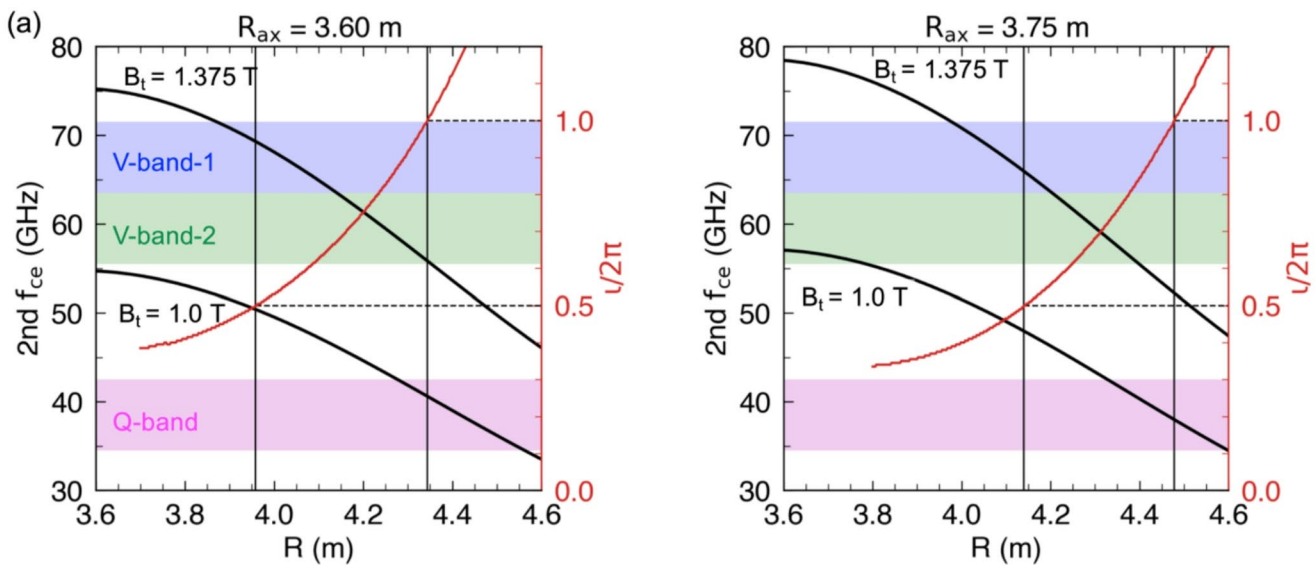


**Fig. 1** Radial profile of second harmonic electron cyclotron frequencies for  $B_t = 1.375$  T and  $B_t = 1.0$  T, with the radial profile of rotational transform  $\iota / 2\pi$  for (a)  $R_{ax} = 3.60$  m and (b)  $R_{ax} = 3.75$  m, at the vertical position  $Z=0$  m. The shaded bands indicate the frequency cover range of the V-band and Q-band receiver

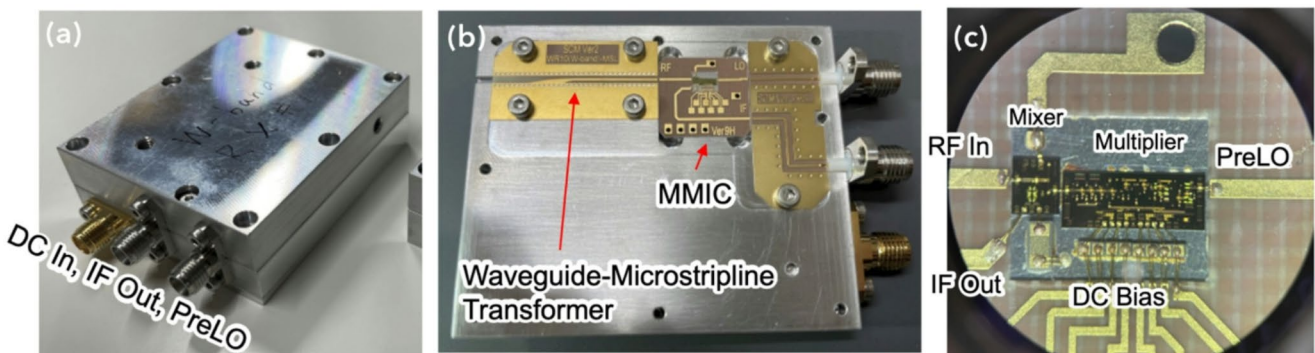


**Fig. 2** Photos of the one-channel of LIA. The exterior of LIA (a), The internal view with the cover removed (b), The detail of MMIC section (c)

In this paper, we introduce the development of the LIA, a key component of the current ECEI system, and the newly installed ECE signal transmission optics to accommodate the LHD deuterium plasma experiment,. Furthermore, we present a preliminary observation of the temperature fluctuation structure of GAM.

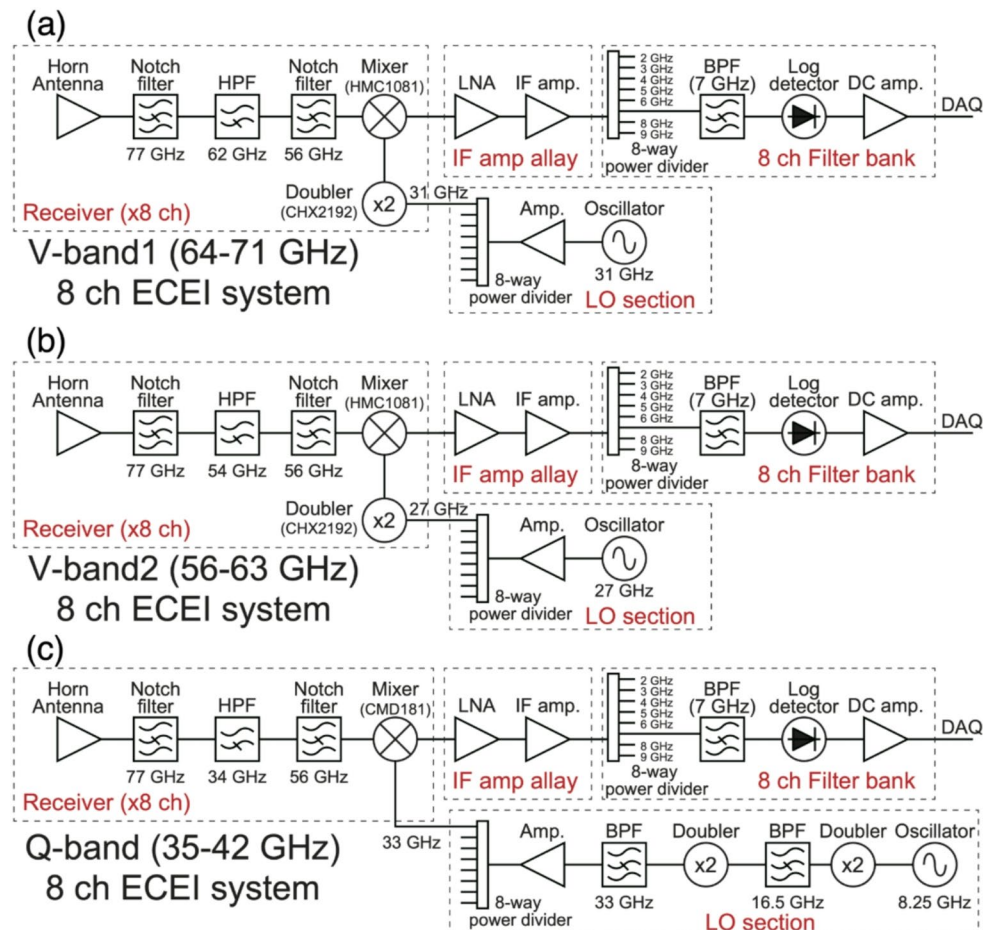
## Heterodyne Radiometer System with Local Integrated Antenna

In the LHD, a heterodyne radiometer system equipped with Horn antenna Mixer Array (HMA) has conventionally served as the receiver for ECEI, offering the advantage of two-dimensional alignment [11]. On the other hand, HMA requires the irradiation of a local oscillation (LO) wave onto the antenna array to generate intermediate frequency(IF) signals, which necessitates both LO optics and a high-power

LO source. The LIA, an upgraded version of HMA, is developed to address this issue and to enable multi-channel measurements [16]. The LIA incorporates an internal LO supply for each channel by utilizing a frequency multiplier integrated circuit. The LO wave for each mixer is directly provided from the Monolithic Microwave IC(MMIC) multiplier. Figure 2 shows photographs of LIA. The pre-LO signals supplied to the multiplier are delivered to the LIA via a coaxial cable. The development of the LIA allows the removal the LO optical component and the high power LO source, resulting in lower costs and reduced space requirements for multi-channelization. Furthermore, this scheme removes the spatial inhomogeneity of sensitivity caused by LO illumination.

We have newly developed V- and Q-band LIA optimized for the ECEI system on LHD. Figure 3 shows the three types of heterodyne detection system: V-band-1, V-band-2 and Q-band with LIA. The ECE signals received by each

**Fig. 3** Heterodyne detection system with LIA of V-band-1 (a), V-band-2 (b), and Q-band (c)



antenna are converted to IF signals and then separated into eight frequency ranges. The center frequencies of the systems are as follows: 64–71 GHz for the V-band-1, 56–63 GHz for the V-band-2, and 35–42 GHz for the Q-band. The corresponding LO frequencies are 62 GHz for V-band-1, 54 GHz for V-band-2, and 33 GHz for Q-band, respectively. In the V-band LIAs, we adopted an approach in which the LO signals are generated by doubling pre-LO frequencies of 31 GHz and 27 GHz, respectively. This differs from previously developed LIA [16], which employ a quadrupler; however, since ECE measurements cover a broad frequency range, the influence of higher harmonics of the pre-LO can cause spurious signals. In this configuration, the third- and fourth-order harmonics of the pre-LO fall outside the detectable bands of the receiver, thereby preventing their contaminations. Note that the ECE signal at the pre-LO frequency is cut off by the high-pass filter. In the Q-band LIA, the MMIC section does not include a frequency multiplier, which also helps to suppress higher-order harmonics. The LO saturation levels of the LIAs are + 5 dBm for the V-band-1, + 10 dBm for V-band-2, and + 17 dBm for the Q-band, all of which are lower than the + 27 dBm required for the HMA. The bandwidth of filter bank is  $\pm 0.4$  GHz at -3 dB and  $\pm 0.5$

GHz at -10 dB around the center frequency, and the quoted center frequencies represent the measured midpoints of the passbands. Notch filters are installed after the horn antenna to reject stray light from the 56 GHz and 77 GHz gyrotrons, protecting the downstream components. The V-band notch filter exhibits attenuation of about 80 dB at 56 GHz and 60 dB at 77 GHz, whereas the Q-band notch filter provides approximately 50 dB at 56 GHz and 55 dB at 77 GHz. These notch filters were originally developed at National Institute for Fusion Science. Design details and test results are documented in Refs [17, 18]. Moreover, the log detector used in each channel provides a wide dynamic range of approximately 45 dB, with a frequency response from DC to 1 MHz (-3 dB).

## ECEI Optics on LHD

This section describes the newly implemented optical system for the present ECEI diagnostics [12]. The previous system has been reported in Ref [11]. The ECEI system is installed at the 4-O port, which corresponds to a horizontally elongated cross-section of the LHD plasma. The

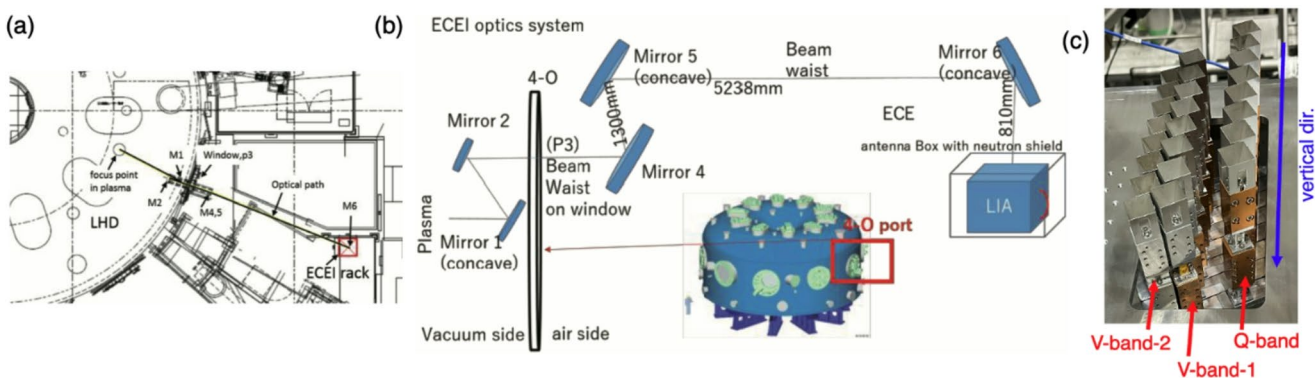


**Fig. 4** (a) Layout of the ECEI optical system. Top view of LHD and the diagnostic stage, showing optical path from plasma to the ECEI rack. Mirrors are indicated as M1, M2, M4, M5, and M6, and P3 is

the vacuum window, (b) Conceptual diagram of the ECEI optical system. (c) Photograph of the installed LIA antenna array. (a) and (b) are reproduced from ref [12]

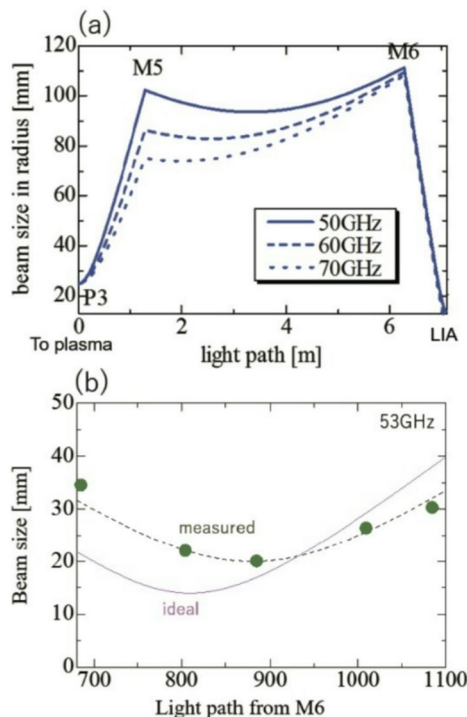


**Fig. 5** (a) Evolution of designed beam radius for 50, 60, 70 GHz. (b) Comparison between measured and designed beam sizes for the 53 GHz beam from M6 to the LIA. The horizontal axis represents the distance from M6, where the 810 mm position corresponds to the LIA position. (Reproduced from ref [12]).

layout of the ECEI optical system is shown in Fig. 4(a). The present optical system was newly designed and installed to meet the requirements of the LHD deuterium plasma experiments, with the LIA antenna array positioned farther from the plasma in order to reduce fast-neutron damage to the semiconductor devices. At a distance of approximately 5 m from the plasma, most fast neutrons are expected to be moderated. The optical system, consisting of five mirrors, transmits the ECE radiation from the plasma to the LIA,

as shown in Fig. 4(b). The installed LIA arrays are shown in Fig. 4(c). The antennas are oriented to detect second-harmonic X-mode ECE radiation, which is not subject to a cutoff along the propagation path and is expected to be optically thick. Mirrors M1 and M2 are located inside the vacuum vessel, while M4, M5 and M6 are installed on the air side. M1, M5, and M6 are concave mirrors, whereas M2 and M4 are flat mirrors. The mirror size and optical path were determined based on the calculations of ECE propagation beam width, treated as Gaussian beam propagation. The spot size at the LIA is designed to correspond to the horn antenna aperture ( $\sim 14$  mm radius). Point P3 corresponds to the vacuum window, whose aperture imposes the most stringent constraint on the optical system; therefore, the beam width is designed so that its waist is located at P3. Figure 5(a) shows the designed beam width evolution along the optical path from the vacuum window (P3) to the LIA. Figure 5(b) shows a comparison between the designed beam width and the beam width measured in a propagation test performed from P3. This discrepancy arises because the assumed 25 mm beam waist at P3 in the design does not exactly match the beam emitted by the horn antenna used in the test, which has a 40 mm  $\times$  30 mm aperture.

## Trial of GAM Structure Observation

This section presents the initial observation of the temperature fluctuation structure of GAM using the ECEI system. GAM is an oscillating branch of zonal flow and has been widely studied because it can suppress turbulent transport by the shearing effect [19]. In addition, energy transfer from energetic particles to bulk ions, mediated by energetic particle driven GAM (EGAM) has attracted attention as

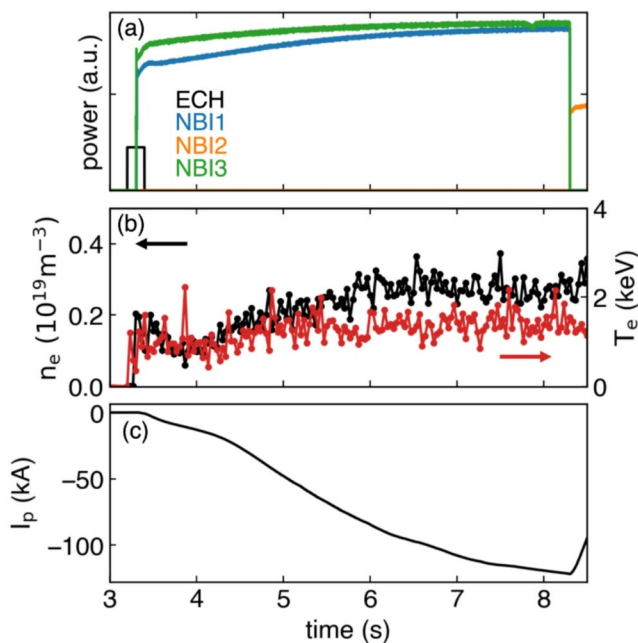
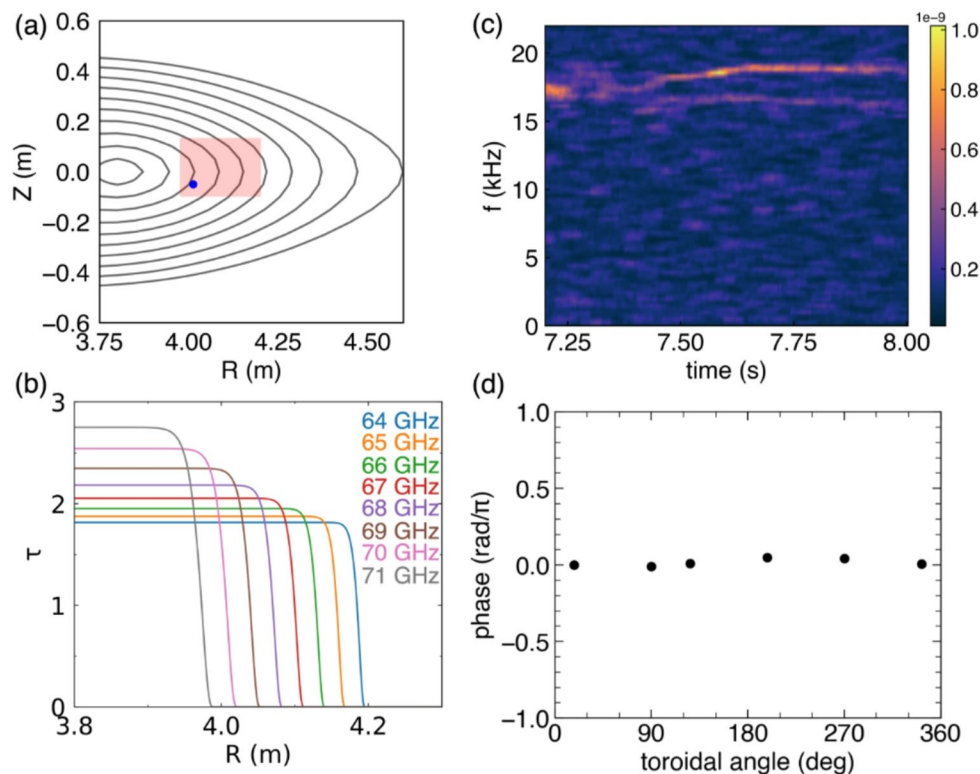


**Fig. 6** Time evolution of heating power (a), electron density and electron temperature around  $R=4.0$  m measured by Thomson scattering (b), plasma current (c)

an ion heating process. EGAM has also been extensively investigated in the LHD [15]. In this study, we employed the V-band-1 module. The experiment was conducted under toroidal magnetic field of  $B_t = 1.375$  T, with the magnetic axis located at 3.75 m on the shot number #178,444. Figure

6 shows the property of the target plasma discharge. After ignition by ECH, the plasma was sustained by counter-injected NBIs (NBI1 and NBI3). Figure 7(a) shows the ECEI measurement region in the poloidal cross-section. The observation covers the range 0.3–0.5 of the normalized effective minor radius  $r_{eff}/a_{99}$ , where  $a_{99}$  denotes the minor radius in which 99% of stored energy is included. As shown in Fig. 7(b), the optical thickness  $\tau$  at the measurement region is greater than one at all channels of center frequencies. Figure 7(c) shows the spectrogram of the ECE signal at 70 GHz. A fluctuation signal at  $f = 18.8$  kHz of EGAM was observed. The toroidal magnetic probe array confirmed that the toroidal mode number of the  $f = 18.8$  kHz fluctuation is zero, as shown in Fig. 7(d). EGAM with a similar frequency has been reported previously [20]. The spatial structure of EGAM oscillation was investigated by correlation analysis using the cross-spectrum. The color maps in Fig. 8 show the real part of the cross-spectrum at  $f = 18.8$  kHz. The cross spectrum at each spatial point was obtained using the signal at the position indicated in Fig. 7(a) as the reference signal. The reference channel was chosen at the position where the GAM signal is strongest. The analysis was performed over a time window from 7.5 to 8.0 s. The real part of cross-spectrum represents both of correlation and phase to the reference signal. By rotating the vector of the cross-spectrum obtained at each spatial point in the complex plane, the oscillation pattern at each phase can be reconstructed. Here, the oscillation over half a period (0 to  $\pi$ ) of the 18.8 kHz

**Fig. 7** (a) Horizontally elongated cross-section. The red-shaded area indicates the measurement region. The contour lines represent the normalized effective minor radius  $r_{eff}/a_{99}$  for every 0.1 increment. (b) Optical thickness at the measurement region with  $z=0$  and  $t=7.7$  s. (c) The spectrogram of the 70 GHz ECE signal at the position marked by the blue dot in (a). (d) Phase differences of magnetic field fluctuation of  $f=18.8$  kHz measured by the toroidal magnetic probe array. The horizontal axis indicates the toroidal angles of the position of the coils, and the vertical axis indicates the phase delay of the fluctuation signal. The error bars are smaller than the symbol size



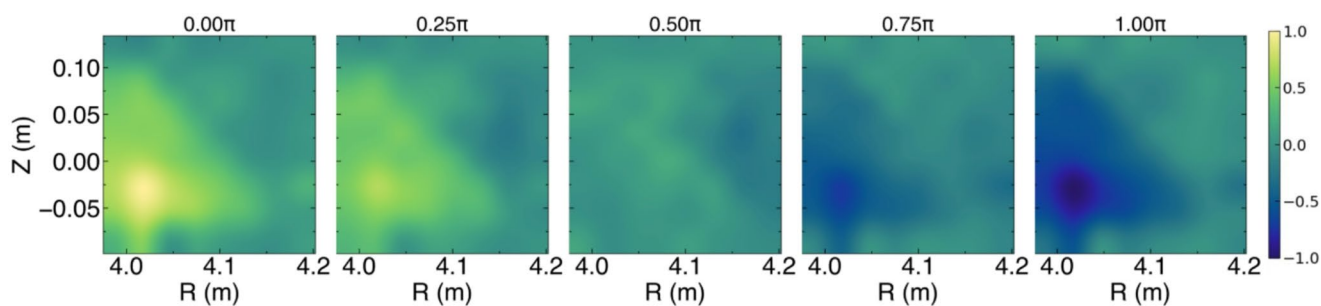


**Fig. 8** The real-part of cross spectrum of 18.8 kHz oscillation at each phase

component is shown. It is clear that the spatial pattern of the temperature fluctuation behaves like a standing wave. While it is known that the density fluctuations of GAMs form a standing wave structure, this observation suggests that the temperature fluctuations also possess similar characteristics. This result is the first observation of the two-dimensional temperature fluctuation structure of EGAM in the LHD and demonstrates the capability of the developed ECEI system.

## Conclusion

The V- and Q-band ECEI systems utilizing LIA has been developed, enabling two-dimensional observation of temperature fluctuations in the LHD. The newly developed V-band receivers have, for the first time, enabled observation of the two-dimensional spatial structure of temperature fluctuations of GAM in LHD plasmas. The successful observation indicates that temperature fluctuations of the GAM exhibit a standing wave structure. A detailed investigations of their spatial structures are expected to contribute to the validation of theoretical and simulation models in the future.

**Acknowledgements** The authors thank the LHD experiment group for their support of this work. One of the authors (D.N.) would like to thank K. Ueda for valuable discussions. This work was partially supported by JAPAN/U.S Cooperation in Fusion Research and Development.

**Author Contributions** D.N. analyzed the data and wrote the main manuscript text. D. K. developed the hardware and prepared Figs. 2 and 3. T.T. and T.N. performed the experiment and contributed to the preparation of the manuscript. All authors reviewed the manuscript.

**Data Availability** The data supporting the findings of this study are available in the LHD experiment data repository at <https://doi.org/10.57451/lhd.analyzed-data>.

## Declarations

**Competing Interests** The authors declare no competing interests.

**Open Access** This article is licensed under a Creative Commons Attribution 4.0 International License, which permits use, sharing, adaptation, distribution and reproduction in any medium or format, as long as you give appropriate credit to the original author(s) and the source, provide a link to the Creative Commons licence, and indicate if changes were made. The images or other third party material in this article are included in the article's Creative Commons licence, unless indicated otherwise in a credit line to the material. If material is not included in the article's Creative Commons licence and your intended use is not permitted by statutory regulation or exceeds the permitted use, you will need to obtain permission directly from the copyright holder. To view a copy of this licence, visit <http://creativecommons.org/licenses/by/4.0/>.

## References

1. H.K. Park, Newly uncovered physics of MHD instabilities using 2-D electron cyclotron emission imaging system in toroidal plasmas. *Adv. Physics: X*. **4**(1), 1633956 (2019)
2. Y. Zhu, J.-H. Yu, M. Chen, B. Tobias, N.C. Luhmann, New trends in microwave imaging diagnostics and application to burning plasma. *IEEE Trans. Plasma Sci.* **47**(5), 2110–2130 (May 2019)
3. H.K. Park et al., Observation of High-Field-Side crash and heat transfer during Sawtooth Oscillation in magnetically confined plasmas. *Phys. Rev. Lett.* **96**(19), 195003 (2006)
4. Y. Zhu et al., W-band system-on-chip electron cyclotron emission imaging system on DIII-D. *Rev. Sci. Instrum.* **91**(9), 093504 (2020)
5. G.S. Yun et al., Quasi 3D ECE imaging system for study of MHD instabilities in KSTAR. *Rev. Sci. Instrum.* **85**(11), 11D820 (2014)
6. I.G.J. Classen et al., Dual array 3D electron cyclotron emission imaging at ASDEX upgrade. *Rev. Sci. Instrum.* **85**, 11 (2014)
7. H.A.N. Kexi et al., Quasi-optical characterization and preliminary experimental results of electron cyclotron emission imaging on HL-3 Tokamak. *Plasma Sci. Technol.* **27**(6), 065101 (2025)
8. B.J. Tobias et al., Fast ion induced shearing of 2D Alfvén eigenmodes measured by electron cyclotron emission imaging. *Phys. Rev. Lett.* **106**(7), 075003 (2011)
9. M.J. Choi et al., Improved accuracy in the Estimation of the tearing mode stability parameters ( $\Delta'$  and  $w_c$ ) using 2D ECEI data in KSTAR. *Nucl. Fusion*. **54**, 083010 (2014)
10. G.S. Yun et al., Two-Dimensional visualization of growth and burst of the Edge-Localized filaments in KSTAR H-Mode plasmas. *Phys. Rev. Lett.* **107**(4), 045004 (2011)
11. D. Kuwahara et al., Development of electron cyclotron emission imaging system on large helical device. *Rev. Sci. Instrum.* **81**, 10 (2010)
12. H. Tsuchiya et al., Installation of new electron cyclotron emission imaging in LHD. *Plasma Fusion Res.* **13**, 3402063–3402063 (2018)

13. Y. Goto et al., Development of the Q-band ECE imaging system in the large helical device. *J. Instrum.* **17**, C01016 (2022)
14. J. Varela et al., Effect of the tangential NBI current drive on the stability of pressure and energetic particle driven MHD modes in LHD plasma. *Nucl. Fusion.* **60**(2), 026016 (2020)
15. T. Ido et al., Identification of the energetic-particle driven GAM in the LHD. *Nucl. Fusion.* **55**(8), 083024 (2015)
16. D. Kuwahara et al., Development of local oscillator integrated antenna array for microwave imaging diagnostics. *J. Instrum.* **10**(12), C12031 (2015)
17. M. Nishiura et al., Q-band high-performance Notch filters at 56 and 77 GHz Notches for versatile fusion plasma diagnostics. *Rev. Sci. Instrum.* **92**(3), 034711 (2021)
18. T. Tokuzawa et al., New Q and V-band ECE radiometer for low magnetic field operation on LHD. *EPJ Web of Conferences.* EDP Sciences, 277(2023)
19. G.D. Conway, I. Andrei, Smolyakov, Takeshi Ido Geodesic Acoust. Modes Magn. Confinement Devices Nuclear Fusion. **62**(1), 013001 (2021)
20. K. Toi et al., Observation of Reversed-Shear Alfvén eigenmodes excited by energetic ions in a helical plasma. *Phys. Rev. Lett.* **105**(14), 145003 (2010)

**Publisher's Note** Springer Nature remains neutral with regard to jurisdictional claims in published maps and institutional affiliations.